Green Chemical Technology

SCIEPublish

Article

Nitric Acid Post-Treatment of Physically Activated Hydrochars: Contrasting Effects on Methylene Blue and Phenol Adsorption

Ghazaleh Chegini [1], Cedric Briens [1] and Dominic Pjontek [1,2,*]

[1] Institute for Chemicals and Fuels from Alternative Resources (ICFAR), Western University, London, ON N6A 3K7, Canada; gchegini@uwo.ca (G.C.); cbriens@uwo.ca (C.B.)

[2] Department of Chemical and Biological Engineering, University of Ottawa, Ottawa, ON K1N 6N5, Canada

* Corresponding author. E-mail: dpjontek@uottawa.ca (D.P.)

Received: 28 July 2026; Revised: 14 August 2026; Accepted: 8 September 2026; Available online: 22 September 2026

ABSTRACT: Hydrochar is a low-cost carbon precursor for water treatment, but its adsorption performance depends on both texture and surface chemistry. This work evaluates whether a nitric acid (HNO_3) post-treatment can direct physically activated hydrochar adsorbents toward a target contaminant class. An industrially produced hydrochar was activated at 800 °C for 2 h under N_2, CO_2, or steam, then treated with 70% HNO_3. Adsorption was evaluated using methylene blue as a representative cationic dye and phenol as a representative aromatic micropollutant. The post-treatment altered surface chemistry rather than texture: total acidic groups increased by 86 to 123% and basic groups decreased by 56 to 66%, lowering the point of zero charge to 4.5–5.3, while Brunauer-Emmett-Teller (BET) surface areas were largely preserved (largest reduction of 14%, most changes below 5%). These changes had opposing consequences for the two adsorbates: methylene blue capacity increased by up to 135%, reaching 264 $mg \cdot g^{-1}$ for the post-treated steam-activated hydrochar, whereas phenol capacity decreased by up to 58% from a maximum of 167 $mg \cdot g^{-1}$ for the same steam-activated char before post-treatment. The HNO_3 post-treatment is therefore selective rather than universally beneficial as it valorizes hydrochar adsorbents for cationic contaminants while reducing their affinity for neutral aromatics.

Keywords: Hydrochar; Nitric acid oxidation; Surface functional groups; Methylene blue; Phenol; Point of zero charge; Water treatment

1. Introduction

Hydrothermal carbonization (HTC), or wet torrefaction, is an active area of research due to its energy efficiency and product yield when compared to conventional dry pyrolysis [1]. HTC is a technology that heats and decomposes wet biomass (e.g., agricultural wastes) under relatively low temperatures (180–350 °C) and elevated pressures (1–5 MPa) in the presence of water. Hydrochar, a carbon-rich, lignite-like solid, is one of the products of HTC and has applications similar to those of biochar, including adsorption of contaminants from water [2], soil amendment for carbon sequestration or fertility enhancement [3,4], fuel and energy storage [5], and catalysis [6,7]. Compared to biochar, hydrochar has a higher volatile

organic compound (VOC) content, which may leach into water and contribute to its contamination [8]. Hydrochar also generally has a lower surface area and pore volume compared to biochar, providing fewer sorption sites for contaminants [9]. This work focuses on the application of hydrochar materials as an adsorbent for contaminant removal in waste water treatment. Phenol and methylene blue are used as representative organic contaminants, where phenol represents low molecular-weight organic micropollutants (e.g., waste streams from petrochemical plants, pharmaceutical manufacturing), while methylene blue is representative of larger organic contaminants (e.g., dyes in textile industries) [10,11]. Methylene blue is a cationic aromatic dye with low biodegradability that is discharged in large volumes and has been associated with adverse health effects; consequently, it is used as a model pollutant to evaluate carbon-based materials for water treatment [12].

Physical activation methods and/or surface chemistry modifications can provide a pathway to tune hydrochar materials based on the desired adsorption properties. Prior work from our group summarized the effect of varying thermal/physical activation methods on the surface area and adsorption capacities for hydrochar samples from different feedstocks [13]; however, the impact of activation method on the surface chemistry of the adsorbents was not discussed. Gas-phase oxidation generally enhances the concentration of hydroxyl (–OH) and carbonyl (R–C=O) surface groups, while liquid-phase oxidation typically increases the number of carboxyl (–COOH) surface groups [14]. Liquid oxidation of carbonaceous materials by inorganic acids has been reported to mainly impact the surface chemistry, rather than the textural properties of the carbons [14]. Nitric acid (HNO_3) is one of the most widely used acids, besides phosphoric and hydrochloric acids. When post-treating carbonaceous materials with HNO_3, minerals are removed, the acidic surface property of the adsorbent is increased, and the hydrophilic nature of the carbon surface is improved [15]. Prior work has shown that acid post-treatment generally decreased the surface area and micropore volume, which resulted in either pore blockage by oxygen functional groups or pore destruction due to severe oxidation [16,17]. Table 1 summarizes prior studies that investigated the use of a HNO_3 post-treatment for carbonaceous materials derived from biomass materials. As expected, all literature reported increases in total acidic groups and decreases in total basic groups. However, each of these studies applied the post-treatment to a single precursor prepared by a single activation route. Because the reported effects are convolved with differences in feedstock, activation method, and activation severity between studies, the extent to which the response to an oxidative post-treatment depends on the preceding physical activation cannot be resolved by comparison across the literature. Applying the same post-treatment to a common hydrochar activated under different atmospheres allows this dependence to be isolated.

Table 1. Selected characteristics from prior investigations on HNO_3 as a post-treatment for biomass/carbon-based adsorbents. Bold values are before the specified post-treatment (Abbreviations: MB—methylene blue, PNP—p-nitrophenol, N/A—not applicable, n.d.—no data).

Biomass	Activation Method	[HNO_3], Time	S_{BET} ($m^2 \cdot g^{-1}$)	V_{total} ($cm^3 \cdot g^{-1}$)	pH_{PZC}	Total Acidic Groups ($mmol \cdot g^{-1}$)	Total Basic Groups ($mmol \cdot g^{-1}$)	Adsorbate Capacity ($mg \cdot g^{-1}$)	Ref.
Olive stone	H_3PO_4 Steam	-	1242	0.56	6.1	0.85	0.4	MB, phenol	455, 32.4	[17]
		2 M, 3 h	1163	0.55	4	1.2	0.1		625, 28.6	
		3 M, 3 h	614	0.29	3.98	1.56	0		667, 24.4	
Orange peels	Hydrothermal	-	34	0.047	6.3	1.70	0.96	MB	59.6	[18]
		70%, 4 h	20	0.042	5.1	2.39	0.49		107	
Weed char	Pyrolysis, 500 °C, 1 h	-	40	0.036	8	1.08	1.11	MB	40	[19]
		65%, 1 h	5	0.006	4	2.27	0.58		161	
Waste tea	H_3PO_4, 450 °C, 1 h	-	1417	1.19	-	0.37	0.41	MB	429	[20]
		20% (*v*/*v*)	644	0.44	-	0.85	0.31		588	
		40% (*v*/*v*)	524	0.29	-	2.06	0.26		684	
Almond shell	CO_2, 835 °C	-	851	0.37	10.4	-	-	PNP, phenol	224, 139	[21]
		N/A, 1 h	817	0.36	3	-	-		154, 76	
Vine shoot	CO_2, 840 °C	-	956	0.44	9.7	-	-	PNP, phenol	238, n.d.	
		N/A, 1 h	646	0.29	2.3	-	-		126, 73	
Rice straw	Pyrolysis, 550 °C, 1 h	-	71	-	9.5	5.6	6.22	MB, phenol	31, 83	[22]
		65%, 3 h	87	-	3	8.9	2.79		39, 67	
Corn cob	Pyrolysis, 500 °C	-	40	0.075	-	-	-	MB, Pb^{2+} mmol/g	n.d., 0.237	[23]
		65%, 1 h	52	0.173	-	-	-		0.225, 0.691	
Corn cob	Steam, 600–850 °C	-	664–700	0.32–0.3	-	-	-	MB, Pb^{2+} mmol/g	0.314–0.722, 0.541–0.43	
		65%, 1 h	577–540	0.36–0.29	-	-	-		0.516–0.788, 0.816–1.13	

For organic contaminants, the adsorption process is mainly governed by electrostatic interactions, pore filling, π-π interactions, hydrogen bonding, and hydrophobic interactions [24]. For instance, the adsorbent total pore volume and pore size distribution impact contaminant adsorption onto adsorbents by pore filling [25], while the adsorbate molecular size dictates its access to the pores based on their pore diameter. The surface chemistry of activated carbons depends on their heteroatom content, primarily their oxygen functional groups, which affect their surface charge, hydrophobicity, and electron density. Upon immersion in an aqueous solution, the carbonaceous adsorbent develops surface charges due to the dissociation of surface groups and/or the adsorption of ions from the solution via electrostatic attraction [26,27]. In cases where oxygen-containing functional groups are not dissociated (e.g., carbon with neutral/positive surface charge), hydrogen bonding can occur between oxygen atoms of the negatively charged organic compounds and the hydrogen of oxygen-containing groups [24]. Hydrophobic interactions have been shown to play a part in the adsorption of non-polar contaminants on the adsorbent surface [28]. For carbonaceous materials with higher aromaticity, usually produced at higher temperatures, the loss of oxygen and hydrogen in the adsorbent leads to lower polarity and higher aromaticity, thus promoting the adsorption of aromatic contaminants by forming π-π interactions between the aromatic ring in the adsorbate and the electron-rich region of the carbon surface [25,29,30]. Direct evidence for these mechanisms has been reported for phenol adsorption on biomass-derived carbons, where π-π interactions between the phenol aromatic ring and the carbon layers, together with electron donor-acceptor complexes involving surface C–C, C–O, and C=O groups, were identified as the dominant contributions, and where the surface charge of the adsorbent measured by zeta potential governed the electrostatic component of uptake [31]. These mechanisms lead to opposing expectations for the two model adsorbates used in this work. An oxidative post-treatment that enriches the surface in acidic oxygen functionalities and lowers the point of zero charge should promote electrostatic attraction and hydrogen bonding with a cationic dye such as methylene blue, while simultaneously reducing the π electron density of the carbon basal planes and increasing surface hydrophilicity, both of which are expected to disfavor the adsorption of a neutral aromatic such as phenol.

The activation study introduced above [13] established that hydrochar activated at 800 °C and 2-h holding times were the most promising for waste-water applications (*i.e.*, based on methylene blue and phenol adsorption); nonetheless, the adsorption capacities of N_2, CO_2, and steam activated hydrochar were approximately 35, 60% and 75%, respectively, of the observed capacity for a coconut based activated carbon. This work aims to determine how the physical activation method and a subsequent HNO_3 post-treatment interact to control the surface chemistry and adsorptive capacity of hydrochar-derived carbons for the same model adsorbates. The produced adsorbents are characterized based on their adsorption capabilities for phenol and methylene blue, the textural properties, and surface chemical characteristics. To our knowledge, this is the first study to determine the impact of a HNO_3 post-treatment for varying physical activation methods used on a common industrially produced hydrochar.

2. Materials and Methods

2.1. Hydrochar

Hydrochar materials were provided by Origin Materials and were generated from a patented process using wood feedstocks. It should be noted that two batches of hydrochar samples were used to produce the studied materials. All pyrolytic hydrochars (*i.e.*, using N_2 for activation) were prepared with batch 1, while all CO_2 and steam-activated hydrochars were produced with batch 2. A comparison of proximate, ultimate analysis, surface area, and porosity characteristics of both batches is provided in prior work [13]. It should be noted that the hydrochar materials were used in the same condition as received, where no additional chemical or mechanical treatment was performed before experiments.

2.2. Hydrochar Activation Methods

Hydrochar activations were carried out in the Jiggle Bed Reactor, developed at the Institute for Chemicals and Fuels from Alternative Resources (ICFAR) specifically for endothermic reactions. The reactor configuration and operation details can be found in prior work [13]. The semi-batch fluidized reactor is made of Inconel, has an inner volume of 80 mL, and is agitated by a pneumatic actuator. A heating rate of 50 °C·min^{-1} was used to reach the final activation temperature for the specified time. Products were then cooled to room temperature at a controlled rate (~125 °C·min^{-1}) under a nitrogen environment and were stored in an airtight container before characterization. All runs were performed at atmospheric pressure.

Pyrolytic hydrochars were produced using N_2 at temperatures ranging from 400 to 900 °C and holding times of 1 and 2 h. CO_2 and steam were also used to produce activated hydrochars at temperatures ranging from 700 to 900 °C and holding times of 1 and 2 h. The performance of each hydrochar-derived carbon was assessed based on its methylene blue and phenol adsorptive capacities. Full details of the hydrochar activation methods are detailed elsewhere [13]. Results indicated that the pyrolytic, CO_2-activated, and steam-activated hydrochars produced at 800 °C and a 2-h holding time were the most promising for waste water applications. These conditions were selected for three reasons. First, the methylene blue and phenol adsorption capacities of both the CO_2 and steam-activated hydrochars increased with activation temperature up to approximately 800 °C, beyond which both capacities reached a plateau, so higher temperatures offered no measurable adsorption benefit. Second, the product yield decreased steadily as temperature increased, so operating beyond this plateau would incur a substantial yield penalty without a corresponding gain in performance. Third, this range is consistent with prior reviews of physical activation, which indicate that temperatures between 700 and 800 °C, with holding times of close to 2 h, produce carbons with the highest surface area and porosity. For the steam-activated hydrochar in particular, the adsorption capacities plateaued above 700 °C with a slight further increase at 800 °C, and the sample produced at 800 °C gave the highest BET surface area (593 m^2·g^{-1}) and the highest capacities for both adsorbates among the physically activated materials, which is why it was carried forward as the most promising precursor for the HNO_3 post-treatment. In this work, the activated hydrochars are referred to as N_2, CO_2, and steam chars and were used as precursors to produce HNO_3-modified carbons.

2.3. HNO_3 Post-Treatment Method

The selected activated hydrochar samples were used for the wet oxidation post-treatment using nitric acid (HNO_3) purchased from Fisher Scientific (Waltham, MA, USA). Table 2 summarizes previous post-treatment methods using HNO_3 as a wet oxidizing agent. In our study, N_2, CO_2, and steam-activated chars were treated with 70% (*w*/*w*) nitric acid. A sample of approximately 1.5 g of activated hydrochar was treated with nitric acid at 80 °C for 6 h, followed by a vacuum filtration step to isolate the solid product. The activated hydrochar was then rinsed with a 1.0 M NaOH solution in the vacuum filtration setup, followed by rinsing with distilled water until the water wash effluent reached a pH of 6–7. It should be noted that the NaOH step was included because an initial rinsing procedure using distilled water alone required large volumes of water to reach an effluent pH of 6–7, which would present scale-up issues. The post-treated samples were then dried in an oven at 110 °C overnight before further measurements.

Table 2. Comparison of prior methods for HNO_3 post-treatment of carbon samples (Abbreviation: n.d.—no data).

Precursor	Post-Treatment Condition			Adsorbate	Reference
	Temperature	Solid Mass	Acid Volume, Concentration		
Commercial activated carbon	Boiling, batch for 3 and 6 h	2 g	100 mL, 5 M	Phenol	[16]
Waste tea	90 °C, reflux	3 g	150 mL, 80%	Methylene blue Phenol	[20]
Commercial activated carbon	Boiling, reflux	9 g	200 mL, 5 M	Phenol Aniline Nitrobenzene	[32]
Hydrochar orange peel	Batch, 4 h	1 g	30 mL, 70%	Methylene blue	[18]
Commercial activated carbon	60 °C, batch, 6 h	1 g	10 mL, 69%	Cu^{2+}	[33]
CO_2 activated oil palm shell	80 °C, reflux, 6 h	50 g	n.d., 10 M	-	[34]
Pyrolytic hydrochar CO_2 activated hydrochar Steam activated hydrochar	80 °C, batch, 6 h	1.5 g	15 mL, 70%	Methylene blue Phenol	This work

2.4. Product Characterization

2.4.1. Surface Area and Porosity

The specific surface areas (S_{BET}) were determined based on the linear region of the isotherms, which ranged between relative pressures (P/P_0) of approximately 0.1 to 0.5 for the studied samples. Measurements used the Brunauer–Emmett–Teller (BET) method by N_2 physisorption at 77 K using a NOVA 1200e (Quantachrome Instrument, Boynton Beach, FL, USA). Pore volumes were calculated from the desorption branch of N_2 isotherms using Barrett–Joyner–Halenda (BJH) theory. Between 0.2–0.3 mg of product was degassed under vacuum and at a temperature of 300 °C for at least 5 h prior to the measurement.

2.4.2. Elemental Analysis

The C, H, N, S, and O content of the samples was determined using a Thermo Flash EA 1112 series analyzer (Thermo Fisher Scientific, Waltham, MA, USA). Samples were analyzed in triplicate, and the results are reported as mean mass percentage of the dry samples, with the observed standard deviations. Oxygen content was calculated by the difference of C, H, N, and S from unit mass, as the ash content was determined to be relatively low for both hydrochar samples (0.6% for batch 1 and 1.7% for batch 2).

2.4.3. Point of Zero Charge Determination

The Point of Zero Charge (PZC) was determined following the method detailed by Balistrieri [35]. The initial pH value (pH_i) of 0.1 M NaCl was adjusted from pH 2 to pH 10 by adding 1 M NaOH or 1 M HCl. A volume of 25 mL of each adjusted solution was then added to 0.05 g of solid samples. The samples were then shaken at 150 rpm for 4 h before the final pH value (pH_f) of the supernatant was recorded. The difference between final and initial pH (ΔpH) was plotted against pH_i, and the point at which ΔpH is equal to 0 was determined as the pH at point zero charge (pH_{PZC}), which is the solution pH at which the carbon surface is neutral [36].

2.4.4. Boehm Titration

The Boehm titration procedure follows the method described by Goertzen et al. [37]. A known mass of hydrochar, between 0.1 to 0.5 g, was added to 30 mL of a 0.05 M NaOH solution. The samples were agitated at room temperature for 24 h and were then filtered using Whatman No. 1 filters to remove the remaining carbon. Aliquots of 10 mL were taken by pipette and were each titrated directly with 0.05 M HCl. NaOH reacts with all functional groups (carboxyls, lactones, and phenols) and therefore provides total

acidity in moles. To determine the basic functional groups, 0.1–0.5 g of each sample was placed in a test tube with 30 mL of 0.05 M HCl solution. The samples were shaken for 24 h, and 10 mL aliquots were taken by pipette and titrated with 0.05 M NaOH. NaOH and HCl solutions were standardized before each experiment. The quantity of acidic or basic surface groups was determined by:

$$n_A = ([NaOH]V_{NaOH} - [HCl]V_{HCl}\frac{V_{NaOH}}{V_a}) \times {}^1/_m \quad (1)$$

$$n_B = ([HCl]'V'_{HCl} - [NaOH]'V'_{NaOH}\frac{V'_{HCL}}{V_a}) \times {}^1/_m \quad (2)$$

where [NaOH] and V_{NaOH} are the concentration and volume of the NaOH added to the samples, n_A ($mol \cdot g^{-1}$) denotes the moles of acid groups on the surface of a unit mass of sample that reacted with the NaOH during the mixing step, m (g) is the mass of the solid sample, V_a (L) is the volume of the aliquot taken from the V_{NaOH} (L), and [HCl] ($mol \cdot L^{-1}$) and V_{HCl} (L) are the concentration and volume of the acid added to the aliquot taken from the original sample. For the determination of basic groups, the same equations were used except [HCl]′ ($mol \cdot L^{-1}$) and V'_{HCl} (L) are the concentration and volume of the HCl mixed with the samples, [NaOH]′ ($mol \cdot L^{-1}$) and V'_{NaOH} (L) are the concentration and volume of the base added to the aliquot taken from the original sample, and n_B ($mol \cdot g^{-1}$) denotes the moles of basic groups on the surface of a unit mass of the sample. In this study, n_A and n_B were reported as total acidic groups and total basic groups in $mmol \cdot g^{-1}$.

2.4.5. Adsorption Isotherms

A volume of 15 mL for different initial concentrations of methylene blue (MB) (ranging between 100 and 1000 $mg \cdot L^{-1}$) and phenol (ranging from 50 to 1000 $mg \cdot L^{-1}$) solutions was placed in a 25 mL test tube. Approximately 0.02 g of solids was added into the solution and agitated at 1000 rpm in a shaker at 30 °C for 48 h. The solutions were then centrifuged, and the final concentration of methylene blue or phenol was measured with a UV-Vis spectrophotometer (Thermo Scientific EVO 220, Waltham, MA, USA) at wavelengths of 664 or 270 nm, respectively. Additional details on the batch adsorption measurements can be found in our prior study [13]. Owing to the limited quantity of activated hydrochar available for the post-treatment step, each point on the reported isotherms represents a single measurement. The reproducibility of the precursor materials and of the adsorption measurement was established in prior work, where the activated hydrochars used here were produced and tested in independent triplicate, giving relative standard deviations below 3% for both methylene blue and phenol uptake at a fixed initial concentration.

Langmuir (Equation (3)) and the Freundlich (Equation (4)) isotherms were employed to describe the adsorptive behavior of methylene blue and phenol as organic contaminants onto the post-treated activated hydrochars. Nonlinear forms of these isotherms are as follows:

$$\text{Langmuir isotherm:} \quad q_e = \frac{K_L q_m C_e}{1+K_L C_e} \quad (3)$$

$$\text{Freundlich isotherm:} \quad q_e = K_F C_e^{1/n} \quad (4)$$

where C_e ($mg \cdot L^{-1}$) is the concentration of the adsorbate in the solution at the equilibrium, q_e ($mg \cdot g^{-1}$) is the amount of contaminant adsorbed on the solid phase at the equilibrium, q_m ($mg \cdot g^{-1}$) is the monolayer adsorption capacity of the adsorbent, K_L ($L \cdot mg^{-1}$) is the Langmuir constant related to the affinity between the adsorbent and contaminant, K_F ($(mg \cdot g^{-1})(mg \cdot L^{-1})^n$) is the Freundlich constant, and n is the Freundlich intensity parameter that reflects the magnitude of the adsorption driving force.

3. Results and Discussion

3.1. Yield, Surface Area, and Porosity

The activated hydrochar yield, BET surface area, and porosity before and after the HNO_3 post-treatment are provided in Table 3. The observed yields before the HNO_3 post-treatment were discussed in a prior study [13], where mass reductions were due to the removal of chemically bound moisture, decomposition of organic materials, and carbon reactions with CO_2 or steam. It should be noted that an attempt to oxidize the raw hydrochar failed due to a near-zero yield, as the solid hydrochar sample mostly dissolved in the concentrated HNO_3, making it nearly impossible to recover the remaining solids. The yields following the HNO_3 post-treatment for CO_2 and steam activation had minor reductions relative to the initial physical activation step, demonstrating that these methods stabilized the adsorbent materials.

The associated N_2 adsorption–desorption isotherms for all samples are provided in Figure 1a,b. All obtained N_2 isotherms are type IV with an H3 hysteresis loop according to the IUPAC classification, confirming that the studied materials are predominantly mesoporous. The type IV designation reflects the capillary condensation step observed at intermediate relative pressures, while the H3 loop is identified by the absence of a saturation plateau at high P/P_0 and by a desorption branch that remains open down to the lower closure limit of the loop, which for N_2 at 77 K occurs near a P/P_0 of 0.42 as a result of cavitation. The isotherms in Figure 1a,b are close between P/P_0 values of approximately 0.4 and 0.5, consistent with this behavior. H3 loops are generally attributed to non-rigid aggregates of plate-like particles and to slit-shaped pores that are not completely filled by the condensate over the measured pressure range, rather than to an ordered network of uniform cylindrical mesopores. This assignment is further supported by the textural data in Table 3, where the average pore diameters of 4.4 to 5.3 nm fall within the mesopore range and micropore volumes account for only 17 to 27% of the total pore volume for the activated samples. Comparable type IV isotherms with H3 hysteresis have been reported for other porous adsorbents and catalysts applied to water treatment [38,39]. The physical activation step produced substantially larger changes in surface area than the subsequent HNO_3 post-treatment. Relative to the raw hydrochar (116 $m^2 \cdot g^{-1}$), activation under N_2, CO_2, and steam increased the BET surface area by factors of 2.5, 3.9, and 5.1, respectively. Under N_2, the increase arises solely from thermal devolatilization, in which trapped pyrolysis products remaining in the pore network from incomplete carbonization of the hydrochar are removed, thereby opening previously blocked porosity. This is reflected in the micropore volume, which increases from zero for the raw hydrochar to 0.071 $cm^3 \cdot g^{-1}$ after N_2 pyrolysis, and in the reduction of the average pore diameter from 11.3 to 5.2 nm as finer porosity develops. Under CO_2 and steam, devolatilization is accompanied by endothermic gasification of the carbon matrix, which both creates new micropores and widens existing ones, producing the higher surface areas and micropore volumes in Table 3. Steam was the more effective activating agent, which is attributed to the smaller molecular size of H_2O relative to CO_2, giving it a higher diffusion rate into the developing pore network and a carbon-steam reaction rate several times greater than that of the Boudouard reaction. The larger molecular size of CO_2 is also consistent with the slightly wider average pore diameter of the CO_2-activated sample (4.7 nm) compared with the steam-activated sample (4.4 nm). These trends are consistent with those reported in prior work [13]. The minor reductions in surface area and porosity observed with the CO_2 and steam activated hydrochars are most likely due to destruction of pore walls because of severe oxidation with nitric acid and/or blocking of micropores with oxygen surface groups located at the pore opening [16,17].

Table 3. BET surface area and porosity of activated and HNO_3 treated hydrochars.

Sample	Yield $\left(\frac{\text{g Product}}{\text{g Hydrochar}}\right)$	S_{BET} ($m^2.g^{-1}$)	Porosity Properties			
			V_t [a] ($cm^3 \cdot g^{-1}$)	V_{micro} [b] ($cm^3 \cdot g^{-1}$)	Micro-Porosity (V_{micro}/V_t,%)	D_P [c] (nm)
Hydrochar	-	116	0.328	0	0	11.3
N_2 (800 °C, 2 h)	0.46	291	0.376	0.071	19	5.2
N_2-HNO_3 (70%, 80 °C, 6 h)	0.33	292	0.387	0.065	17	5.3
CO_2 (800 °C, 2 h)	0.30	455	0.528	0.127	24	4.7
CO_2-HNO_3 (70%, 80 °C, 6 h)	0.28	450	0.513	0.125	24	4.6
Steam (800 °C, 2 h)	0.31	593	0.651	0.174	27	4.4
Steam-HNO_3 (70%, 80 °C, 6 h)	0.26	509	0.557	0.148	27	4.4

[a] V_t—total pore volume (P/P_0 = 0.99). [b] V_{micro}—micropore volume (determined by the t-plot method). [c] D_p—average pore diameter.

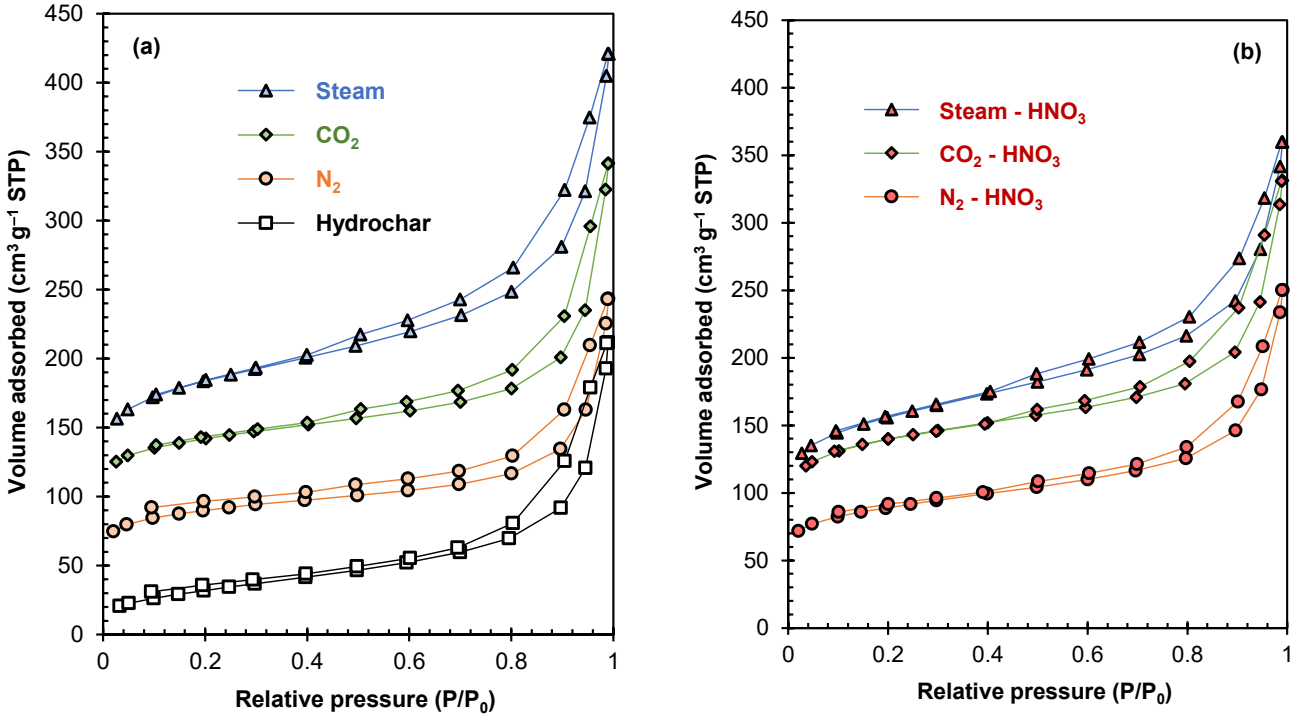

Figure 1. N_2 adsorption–desorption isotherms for (**a**) the hydrochar following physical activation and (**b**) after the HNO_3 post-treatment.

3.2. Elemental Analysis

The degree of carbonization and aromaticity can be estimated from the H/C molar ratio [40,41]; the (O+N)/C ratio indicates the char polarity, and the O/C ratio indicates the degree of hydrophilicity of the adsorbent [42,43]. Table 4 provides the changes in the C, H, N, and O composition of the carbonaceous materials before and after the HNO_3 treatment. The sulfur content is not mentioned in this table but is accounted for when calculating oxygen by difference.

The carbon content decreased after HNO_3 treatment for all samples, whereas the oxygen and nitrogen contents increased. This is mainly due to the corresponding increase in oxygen-containing functional groups involving carboxylic, phenolic, and nitro moieties on the surface [44,45], and/or an increase in NO_2 or NO_3 groups resulting directly from HNO_3 [46]. The reduced H/C molar ratios following pyrolysis, CO_2, and

steam activation suggest that activated hydrochars contained reduced amounts of the original organic residues and a higher degree of carbonization [42]. The N_2 pyrolysis sample at 800 °C offers a higher H/C ratio and lower O/C and (O+N)/C ratios than those produced using oxidative gases (*i.e.*, CO_2 and steam), suggesting decreased aromaticity accompanied by decreased polarity. The O/C molar ratios for the HNO_3 treated samples were all higher than that of the original samples, suggesting greater hydrophilicity for the post-treated carbons. The HNO_3 post-treated hydrochars also had a higher polarity index [(O+N)/C] than the originals, suggesting a higher concentration of surface polar functional groups (C–OH and COOH) [47].

Table 4. Elemental analysis of activated and HNO_3 treated hydrochars.

Sample	Ultimate Analysis (wt%)				Atomic Ratios		
	C	H	N	O [a]	H/C	O/C	(O+N)/C
Hydrochar	62.9 ± 0.1	4.3 ± 0.0	0.2 ± 0.1	32.3 ± 0.1	0.81	0.39	0.39
N_2 (800 °C, 2 h)	86.1 ± 1.3	1.9 ± 0.2	0.3 ± 0.1	11.3 ± 1.7	0.27	0.10	0.10
N_2-HNO_3 (70%, 80 °C, 6 h)	65.4 ± 0.8	1.8 ± 0.0	1.3 ± 0.0	31.2 ± 0.9	0.33	0.36	0.37
CO_2 (800 °C, 2 h)	82.2 ± 0.5	1.4 ± 0.0	0.2 ± 0.0	15.9 ± 0.5	0.20	0.15	0.15
CO_2-HNO_3 (70%, 80 °C, 6 h)	55.9 ± 0.9	1.6 ± 0.0	2.2 ± 0.1	40.0 ± 1.0	0.35	0.54	0.57
Steam (800 °C, 2 h)	82.3 ± 1.6	1.6 ± 0.1	0.1 ± 0.0	15.7 ± 1.6	0.23	0.14	0.14
Steam-HNO_3 (70%, 80 °C, 6 h)	67.3 ± 0.2	1.7 ± 0.0	1.3 ± 0.1	29.3 ± 0.2	0.29	0.33	0.34

[a] calculated by difference.

3.3. Surface Chemistry

The pH at which the adsorbent surface charge takes a zero value is defined as the point of zero charge (pH_{pzc}). Figure 2 shows the determination of the pH_{pzc} for activated and HNO_3 post-treated hydrochar samples. At the pH_{pzc}, the charge of the positive surface sites is equal to that of the negative ones. Knowing the pH_{pzc} allows one to hypothesize the ionization of functional groups and their interaction with anionic and cationic species in solution. For solutions where $pH > pH_{pzc}$, the adsorbent surface is negatively charged and could interact with cationic species, while at $pH < pH_{pzc}$, the solid surface is positively charged and could interact with negative species [48]. Activated carbons are believed to be amphoteric materials, which have both acidic and basic surface functional groups [49].

Table 5 provides the pH_{pzc} and the total acidic/basic groups of activated hydrochar before and after the HNO_3 treatment. The pH_{ads} were measured as the initial pH of a suspension containing 0.02 g of adsorbent in 15 mL of DI water. All samples in water have a pH_{ads} value higher than the pH_{pzc}, suggesting that they have a negatively charged surface when placed in the adsorption solution. The higher the difference, the more the surface is negatively charged.

Past studies have shown that an HNO_3 post-treatment prioritizes acidic groups in the following order: carboxylic > lactonic > phenolic groups [16,18]. This notion was corroborated by a higher oxygen content and a higher O/C ratio, suggesting that carboxyl groups are the dominant polar functional groups in the acidic fractions [50]. Table 5 shows that N_2 pyrolysis activation significantly reduced the number of acidic functional groups, confirming the changes in the O/C ratio of the samples in Table 4. For CO_2 and steam activation, total basic groups increased by approximately 40% after activation, while acidic groups were reduced by 10 to 20%. CO_2 activation seemed to favor the production of oxygen functional groups, evident from both Tables 3 and 4, and in agreement with prior work [51,52]. Relative to the pristine samples, the wet oxidation post-treatment with nitric acid removed basic functional groups from the carbon surface.

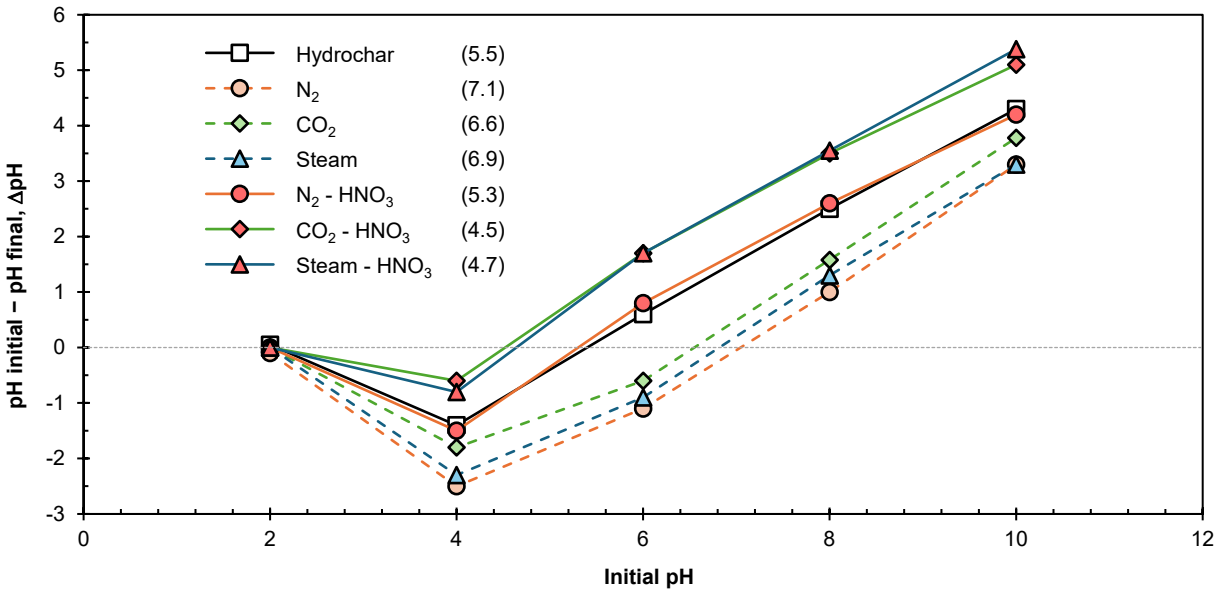

Figure 2. Point of zero charge determination of hydrochar derived samples. Activated samples before (dashed lines) and after nitric acid post-treatment (solid lines, red symbols). Values in parentheses provide the pH_{pzc} for each sample.

Table 5. Total acidic (n_A) and basic groups (n_B) of hydrochar and its derived porous carbons determined by the Boehm titration.

Sample	pH_{pzc}	pH_{ads} [a]	n_A (mmol·g^{-1})	n_B (mmol·g^{-1})
Hydrochar	5.5	5.7	1.81	0.35
N_2 (800 °C, 2 h)	7.1	7.4	0.95	0.43
N_2-HNO_3 (70%, 80 °C, 6 h)	5.3	6.0	2.12	0.19
CO_2 (800 °C, 2 h)	6.6	7.1	1.62	0.5
CO_2-HNO_3 (70%, 80 °C, 6 h)	4.5	5.3	3.01	0.17
Steam (800 °C, 2 h)	6.9	7.3	1.46	0.52
Steam-HNO_3 (70%, 80 °C, 6 h)	4.7	5.4	2.89	0.22

[a] pH of 0.02 g solid in 15 mL DI-water; pH of DI-water = 6.7.

3.4. Contaminant Adsorption

3.4.1. Methylene Blue Isotherms

Adsorption isotherms of the hydrochar-derived carbons before and after the HNO_3 post-treatment are presented in Figure 3. The Langmuir and Freundlich isotherms were fitted to the experimental data, and the model parameters are summarized in Table 6. As individual isotherm points were not replicated, the fitted Langmuir and Freundlich parameters are reported as best-fit values without associated confidence intervals. The differences between samples are nonetheless substantially larger than the measurement variability reported for these materials in prior work, and the coefficients of determination for the Langmuir fits exceeded 0.99 for all samples. The Langmuir model provided a better fit for the experimental data, suggesting that the studied samples have homogeneously distributed active sites with monolayer methylene blue coverage. This also suggests that the added surface functional groups are evenly distributed on the carbon interface. The order of adsorption capacity is steam-HNO_3 > CO_2-HNO_3 > steam > CO_2 > N_2-HNO_3 > N_2 > hydrochar. For all activated hydrochars, the HNO_3 post-treatment increased the methylene blue adsorption capacities by comparable absolute amounts (*i.e.*, increasing by 70 to 90 mg·g^{-1}). Hence, the rankings between the studied activation methods remained the same following the post-treatment.

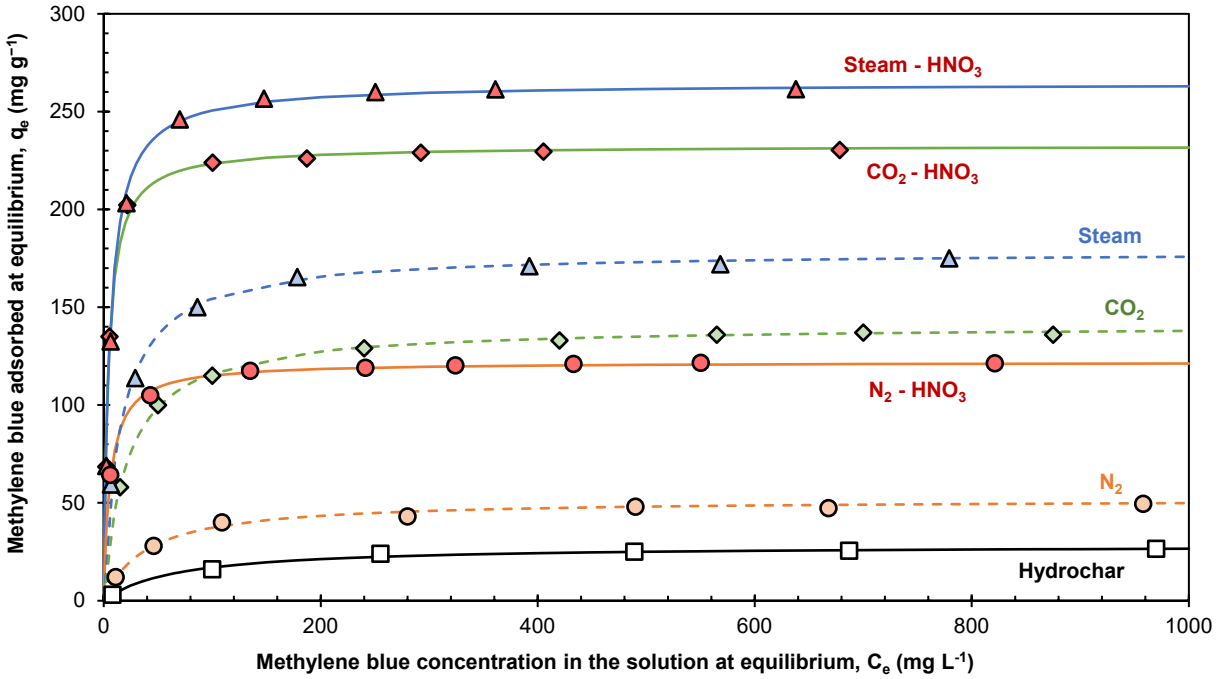

Figure 3. Methylene blue adsorption isotherms on activated hydrochars produced at 800 °C and 2-h holding time before (dashed lines) and after HNO_3 post-treatment (solid lines, red symbols). Lines represent the fitted Langmuir isotherm model.

Comparing the adsorption capacities with the surface areas reported in Table 3, the HNO_3 post-treated materials show an increased adsorption capacity towards methylene blue, despite a slight reduction in surface and porosity characteristics. This is most likely due to the added acidic functional groups onto the surface, as methylene blue is a cationic dye and is dissociated in water to form a positive amino group (R_2N^+). Under the studied experimental adsorption conditions, all investigated samples have negatively charged surfaces ($pH_{ads} > pH_{PZC}$), shown in Table 5, which favors the MB adsorption through electrostatic forces. The post-treatment does not reverse the sign of this charge but increases its magnitude: the difference between pH_{ads} and pH_{PZC} rises from 0.3 to 0.5 for the physically activated samples to 0.7 to 0.8 after the HNO_3 post-treatment, while the density of ionizable acidic groups increases by 86 to 123%. A more strongly negative surface, bearing a higher density of dissociated acidic sites, therefore increases the electrostatic attraction towards the methylene blue cation, which is consistent with the observed increase in maximum adsorption capacity from 47 to 135%. Phenol, in contrast, remains predominantly in its neutral molecular form below its pK_a of 9.9 and gains no comparable electrostatic benefit, while the same surface oxidation reduces the π electron density of the basal planes available for interaction with the aromatic ring. Previous studies have reported similar dye adsorption behavior for other carbonaceous materials [18,19,53].

Table 6. Adsorption parameters of MB on modified pyrolytic and activated hydrochars for Langmuir and the Freundlich models.

Sample	Langmuir Parameters			Freundlich Parameters		
	K_L (L·mg^{-1})	q_m (mg·g^{-1})	R^2	K_F	1/*n*	R^2
Hydrochar	0.015	28	0.99	1.42	0.46	0.92
N_2 (800 °C, 2 h)	0.026	52	0.99	7.65	0.30	0.87
N_2-HNO_3 (70%, 80 °C, 6 h)	0.168	122	0.99	57.9	0.12	0.84
CO_2 (800 °C, 2 h)	0.047	141	0.99	42.1	0.19	0.85
CO_2-HNO_3 (70%, 80 °C, 6 h)	0.244	233	0.99	85.5	0.18	0.75
Steam (800 °C, 2 h)	0.064	179	0.99	49.0	0.21	0.86
Steam-HNO_3 (70%, 80 °C, 6 h)	0.181	264	0.99	80.7	0.22	0.82

3.4.2. Phenol Isotherms

Phenol adsorption isotherms on activated hydrochars before and after the HNO_3 post-treatment are provided in Figure 4. The Langmuir and Freundlich isotherms were again fitted to the experimental data, and their parameters are summarized in Table 7. Similar to MB adsorption, the Langmuir isotherm model fitted the experimental data well, meaning the studied hydrochars have homogeneously distributed active sites with monolayer adsorption. The order of phenol adsorption capacity is steam > CO_2 > steam-HNO_3 > N_2 > CO_2-HNO_3 > hydrochar > N_2-HNO_3. For all activated hydrochars, the HNO_3 post-treatment decreased the phenol adsorption capacities by comparable absolute amounts (*i.e.*, reduced by 50 to 70 $mg \cdot g^{-1}$). Hence, the rankings between the studied activation methods remained the same following the post-treatment.

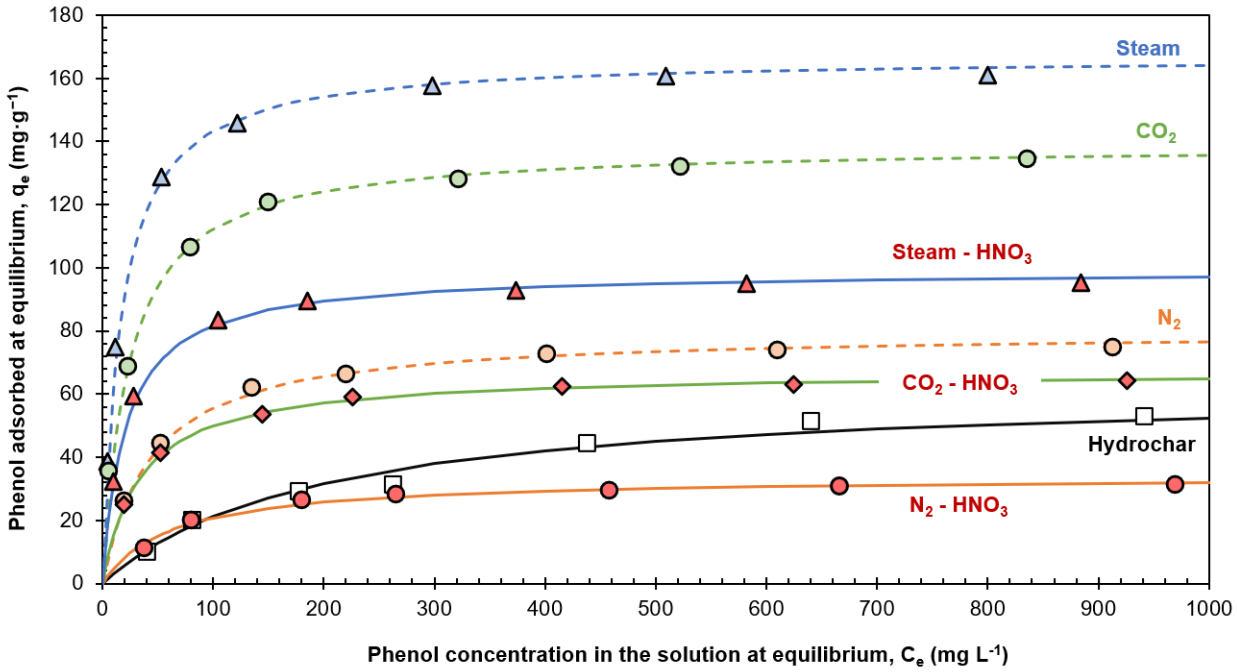

Figure 4. Phenol adsorption isotherms for activated hydrochars produced at 800 °C and 2-h holding time before (dashed lines) and after (solid lines, red symbols) HNO_3 post-treatment. Lines represent a fitted Langmuir isotherm.

Table 7. Adsorption parameters of phenol on modified pyrolytic and activated hydrochars for Langmuir and Freundlich models.

Sample	Langmuir Parameters			Freundlich Parameters		
	K_L ($L \cdot mg^{-1}$)	q_m ($mg \cdot g^{-1}$)	R^2	K_F	$1/n$	R^2
Hydrochar	0.005	63	0.99	2.89	0.37	0.93
N_2 (800 °C, 2 h)	0.023	80	0.99	16.0	0.24	0.86
N_2-HNO_3 (70%, 80 °C, 6 h)	0.016	34	0.99	5.8	0.26	0.81
CO_2 (800 °C, 2 h)	0.042	139	0.99	30.0	0.24	0.86
CO_2-HNO_3 (70%, 80 °C, 6 h)	0.029	67	0.99	16.6	0.21	0.85
Steam (800 °C, 2 h)	0.061	167	0.99	37.9	0.23	0.83
Steam-HNO_3 (70%, 80 °C, 6 h)	0.047	99	0.99	26.6	0.20	0.81

Compared to the activated hydrochar samples, the HNO_3 post-treatment reduced the adsorption capacity and affinity towards phenol, as seen from the maximum adsorption capacities (q_m) and Langmuir constants (K_L). Contrary to the MB adsorption, the HNO_3 treatment was detrimental to phenol adsorption capacity. Although the post-treatment slightly reduced the hydrochar surface areas, the magnitude is insufficient to explain the reduced adsorption capacity. This can be particularly observed for the N_2 and N_2-HNO_3 samples, where the BET surface area is essentially the same, yet the adsorptive capacity is

significantly less after the post-treatment. Since phenol is considered a weak acid, its adsorption should be enhanced in samples with higher basic and lower acidic surface functional groups. Referring to Table 5, the large increase in acidic groups on HNO_3 post-treated samples results in a dramatic drop in phenol adsorption due to these repulsive forces. Similar results have been mentioned by other studies [16,17,19].

3.4.3. Adsorption Discussion

The adsorption of organic contaminants on activated and post-treated hydrochars results from the following phenomena: (a) hydrogen bonding, (b) π-π interaction, (c) electrostatic interaction, (d) pore-filling, and (e) van der Waals forces [24]. Figure 5 illustrates potential adsorption pathways for methylene blue and phenol on the studied hydrochar materials.

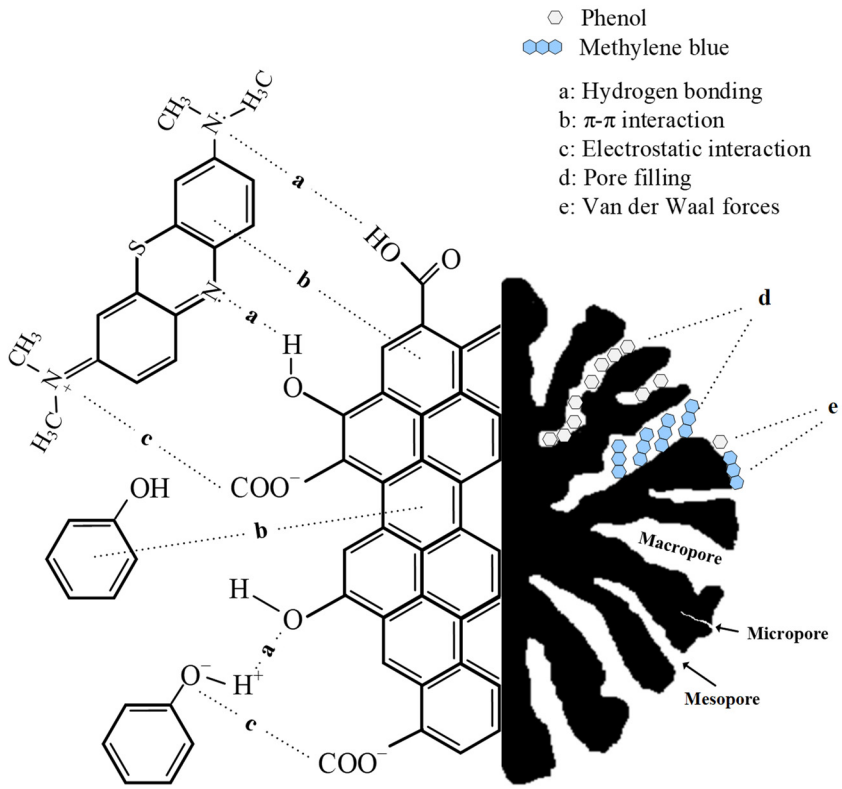

Figure 5. Potential adsorption pathways for methylene blue and phenol on activated hydrochars. Dashed lines illustrate relevant adsorption mechanisms between adsorbates and a hypothetical activated carbon surface.

The van der Waals and pore-filling adsorption mechanisms mainly involve physical adsorption. Based on the Langmuir isotherm fit for both MB and phenol, monolayer coverage can be assumed. According to multi-point BET analysis, at very low relative pressures, N_2 gas is adsorbed in a monolayer formation, S_{BET} is representative of monolayer surface area [54]. The maximum monolayer adsorption of MB and phenol can therefore be estimated from the measured S_{BET} as follows:

$$q_m(\mathrm{mg/g}) = \frac{S_{BET}(\mathrm{m^2/g}) \times MW(\mathrm{mg/mol})}{\sigma\ (\mathrm{m^2}) \times N_{AV}} \quad (5)$$

where MW is the molecular weight, σ is the molecular area of the adsorbate, and N_{AV} is the Avogadro number. The molecular weights of phenol and methylene blue are 94 and 320 $g \cdot mol^{-1}$, and the molecular areas are 0.437 and 1.32 nm^2, respectively [55,56]. Table 8 compares the estimated monolayer coverage based on the BET surface area with the maximum capacity predicted by the fitted Langmuir isotherm model.

HNO_3-modified materials have a similar or slightly reduced specific surface area, yet they show increased MB adsorption and decreased phenol adsorption capacities, respectively.

Table 8. Phenol and MB adsorption capacity based on experimental data and BET surface area.

Sample	S_{BET} ($m^2 \cdot g^{-1}$)	Langmuir Monolayer ($mg \cdot g^{-1}$)		BET Estimated Monolayer ($mg \cdot g^{-1}$)		Langmuir Capacity / BET Based Capacity	
		Phenol	Methylene Blue	Phenol	Methylene Blue	Phenol	Methylene Blue
Hydrochar	116	63	28	41	47	1.5	0.6
N_2 (800 °C, 2 h)	291	80	52	104	119	0.8	0.4
N_2-HNO_3 (70%, 80 °C, 6 h)	292	34	122	104	119	0.3	1.0
CO_2 (800 °C, 2 h)	455	139	141	163	186	0.9	0.8
CO_2-HNO_3 (70%, 80 °C, 6 h)	450	67	233	161	184	0.4	1.3
Steam (800 °C, 2 h)	593	167	179	212	242	0.8	0.7
Steam-HNO_3 (70%, 80 °C, 6 h)	509	99	264	182	208	0.5	1.3

The adsorption estimates of MB based on the BET surface area are lower than the experimental data; thus, van der Waals forces and pore-filling mechanisms are not solely responsible for the higher adsorption of MB on modified carbons. Other studies regarding HNO_3 modified carbons have reported similar observations [19,20,57]. The π-π interactions between the MB aromatic rings and carbon aromatic structures (*i.e.*, hydrophobic interactions) can contribute to the adsorption capacity changes; however, the increasing acidic group concentrations decrease the electron density at the carbon surface, causing a weaker interaction between delocalized π-electrons [18]. This mechanism, therefore, could not be causing the greater MB adsorption on acid-modified carbons. Another possible mechanism is the formation of hydrogen bonds between the heteroatoms (N or S) in the aromatic ring of MB and the hydrogen atoms in the surface carboxylic and phenolic groups (*i.e.*, the major acidic functional groups). Since the modified carbons have higher acidic groups, it is likely that this mechanism plays an important role in MB adsorption [18,58].

Another key consideration is electrostatic interactions. All hydrochars have pH_{PZC} values less than the pH of the adsorption process (pH_{ads}), thus the overall surface charge is negative. The pKa values of acidic groups are 2–4 for carboxyls and 4–7 for lactones. It can thus be assumed that the majority of these functional groups exist in their deprotonated form at the batch adsorption pH, thereby acting as additional binding sites for MB cations via electrostatic interactions [59]. Carbon materials with a higher degree of deprotonated oxygenated surfaces have a stronger negative charge, indicated from the difference between the pH_{ads} and pH_{PZC} [60]. HNO_3 modified carbons thus have higher negative charges than unmodified samples. The electrostatic forces between the deprotonated acidic surface groups of carbons ($–COO^-$) and MB^+ have likely been improved with the HNO_3 post-treatment. The orientation of MB molecules adsorbed on active sites can also be affected by the strength of the electrostatic forces [20]. MB cations are likely located randomly on the hydrochar active sites before post-treatment due to weaker electrostatic forces; however, the formation of acidic groups on the carbon surfaces increases electrostatic attraction, potentially leading to molecular stacking and increasing adsorption capacity above monolayer coverage predictions [61,62]. Previous studies have reported similar effects of hydrogen bond and electrostatic attraction for cationic dye adsorption on other carbonaceous materials [18,19,53].

Past studies have shown that phenol adsorption is dependent on both the adsorbent porosity and the presence of surface groups [63,64]. The solution pH values in this study were always lower than the phenol pKa (9.95), causing phenol to remain in solution predominantly in the molecular state (*i.e.*, not dissociated to ions) [32]. The adsorption mechanisms of molecular phenol onto carbonaceous materials typically

include: (i) pore filling, (ii) π–π interactions, (iii) competitive adsorption of solvent molecules [65–67]. The π–π interaction mechanism mainly exists between the π electrons in the phenol aromatic rings and the delocalized π electrons in the basal planes of carbons [63]. Oxygen atoms bound to the carbon can decrease the π electron density and weaken the dispersion forces between the phenol π electron ring and surface π electrons [68]. This loss of π electron density can therefore reduce the number of sites available for phenol adsorption [69]. Prior studies have also observed a decrease in phenol adsorption capacity with increasing surface oxygen content in carbon materials [68,70]. This suggests that the π-π interactions could dominate phenol adsorption on the carbon surface. Comparing the data from carbon polarity ([O+N]/C) and hydrophilicity (O/C) provided in Table 4, HNO_3 post-treated samples clearly have increased polarity and hydrophilicity. Although the stronger electronegativity of the oxygen atom in the O–H bond makes phenol polar, its polarity compared to the water solvent is much lower. This can cause competitive adsorption between water and phenol on hydrophilic surfaces. Water can form hydrogen bonds on the carbon surface, potentially blocking the passage of phenol molecules to micropores [32]. Although the isotherms in this study were measured at a single temperature and therefore do not permit the determination of adsorption enthalpy and entropy, the fitted Langmuir constants provide a measure of the relative affinity between each adsorbent and adsorbate. For methylene blue, K_L increased by factors of 6.5, 5.2, and 2.8 for the N_2, CO_2, and steam series following the HNO_3 post-treatment, whereas for phenol, it decreased in all cases. The post-treatment, therefore, alters not only the number of accessible adsorption sites, reflected in q_m, but also the strength of the adsorbate-surface interaction, and it does so in opposite directions for the two contaminants. This is consistent with reports that phenol adsorption on biomass-derived carbons is a physisorption-dominated, exothermic process governed largely by π-π interactions, which the introduction of acidic oxygen functionalities disrupts [31]. Two practical considerations follow from the mechanistic differences described above. First, because methylene blue adsorption on the post-treated hydrochars is driven substantially by electrostatic attraction between deprotonated acidic groups and the dye cation, it would be expected to show greater sensitivity to solution ionic strength than phenol adsorption, since dissolved electrolytes screen the surface charge. Phenol, adsorbed predominantly in its neutral molecular form through π-π interactions, should be comparatively insensitive, as has been reported for phenol adsorption on biomass-derived carbons at NaCl concentrations up to 1 M [31]. The net effect for methylene blue is less predictable, as charge screening and the reduced dye solubility associated with increasing electrolyte concentration act in opposite directions. Second, the surface chemistry that enhances methylene blue uptake also constrains the options for adsorbent regeneration. The carboxylic and lactonic groups responsible for the enhancement decompose at moderate temperatures, so thermal regeneration would be expected to remove the functionality introduced by the post-treatment. Regeneration by acid washing, which would protonate the surface carboxylates and release the adsorbed dye cation, is therefore the more plausible route for these materials and warrants dedicated study. Taken together, these observations indicate that the HNO_3 post-treatment operates almost entirely through surface chemistry rather than texture, and that the opposing responses of the two adsorbates are a necessary consequence of a single change rather than two independent effects. The post-treatment preserved the BET surface area to within 14%, yet altered the maximum adsorption capacities by −58 to +135%, so the number of accessible sites cannot account for the observed behavior. What changed instead was the character of those sites. Oxidation simultaneously increases the density of ionizable acidic groups and decreases the π electron density of the carbon basal planes, and these two consequences cannot be decoupled. Methylene blue, which is present as a cation, responds to the first: the greater density of deprotonated carboxylates increases electrostatic attraction, and the resulting capacities exceed the monolayer coverage estimated from the BET surface area, consistent with adsorption beyond a single molecular layer. Phenol, which remains neutral below its pK_a, responds to the second: the loss of π electron density weakens the dispersive interaction with the aromatic ring, while the increased surface hydrophilicity promotes competitive adsorption of water. An oxidative post-treatment is therefore

not a general improvement to a carbon adsorbent, but a means of selecting between contaminant classes, and a comparable trade-off should be expected whenever oxidation is used to target cationic dyes in waters that also contain neutral phenolic compounds.

Understanding the impact of the HNO_3 post-treatment on the adsorption for both model contaminants provides insight into potential improvements based on surface modifications. Phenol is a building block for many pharmaceuticals, pesticides, and polycyclic aromatic hydrocarbons. Research has shown that oxidation has a similar impact on the adsorption capacities of some phenolics, including p-nitrophenol, p-chlorophenol [21,71,72], aniline, and nitrobenzene [32]. In all these studies, oxidation reduced the removal efficiency of the phenolic contaminants from water. The increased acidic groups on the carbons following oxidation post-treatment also resulted in the repulsion of aromatic contaminants, instead favoring the adsorption of water. Methylene blue, on the other hand, is representative of dye contaminants in water. Methylene blue readily dissociates in water, resulting in a positively charged ion. There is thus a considerable influence of electrostatic interactions between the dye adsorbate and the carbon surface. An oxidative post-treatment increases the number of O-containing groups and reduces the pH_{PZC}, which, at solution pH values higher than pH_{PZC}, results in negatively charged carbons. Our MB adsorption observations are in agreement with past studies, showing that oxidation using HNO_3, H_2O_2, or H_3PO_4 will favor the adsorption of basic dyes such as methylene blue, crystal violet, rhodamine B, Acridine Orange, and azure b [20,73–75]. Conversely, oxidative post-treatments will be unfavorable for anionic/acidic and reactive dyes [73,76,77] due to repulsion from the negative surface and reduced π-π interactions of the aromatic structure of the dye with the carbon surface.

4. Conclusions

The HNO_3 post-treatment increased acidic functional groups by 123%, 86%, and 98% and decreased basic groups by 56%, 66%, and 58% for N_2, CO_2, and steam-activated hydrochars, respectively. This post-treatment enhanced methylene blue adsorption capacities by 135%, 65%, and 47% for the N_2, CO_2, and steam-activated hydrochars, respectively. Conversely, the HNO_3 post-treatment had a detrimental effect on the adsorption capacities of phenol. Despite a high acid concentration (70%) during the wet oxidation treatment, the BET surface area and pore sizes remained generally intact, where the largest surface area reduction was for the steam-activated hydrochar with a 14% decrease. This study demonstrates that an HNO_3 post-treatment can further valorize hydrochar adsorbents for the removal of cationic contaminants.

Several aspects were beyond the scope of the present study and are recommended for future work. Electrokinetic characterization by zeta potential would complement the point of zero charge measurements reported here by providing the magnitude of the surface potential and its full pH dependence. Isotherms measured at several temperatures would allow the adsorption enthalpy and entropy to be determined and would establish whether the contrasting responses of the two adsorbates are also reflected in the thermodynamics of adsorption. Adsorption experiments at varying ionic strength would test the expectation that the electrostatically driven uptake of methylene blue is more sensitive to dissolved electrolytes than that of neutral phenol. Finally, regeneration and reuse studies are needed to establish the operating life of these adsorbents, with particular attention to whether the acidic surface groups introduced by the HNO_3 post-treatment can be preserved through repeated adsorption and desorption cycles.

Statement of the Use of Generative AI and AI-Assisted Technologies in the Writing Process

The authors used Claude to improve the language, grammar, and readability of the manuscript. The authors reviewed and edited the content as needed and take full responsibility for the content of the published article.

Acknowledgments

The authors would like to acknowledge MITACS Canada (Grant number IT12425), Origin Materials, and the Faculty of Engineering at the University of Western Ontario for financial support of this study.

Author Contributions

All authors contributed to the study conception and design. Material preparation and data collection were performed by G.C., while analysis was performed by all authors. The first draft of the manuscript was written by G.C. and all authors reviewed and commented on updated versions of the manuscript. All authors have read and approved the final manuscript. All authors agree to be accountable for all aspects of the manuscript.

Ethics Statement

Not applicable.

Informed Consent Statement

Not applicable.

Data Availability Statement

The data that support the findings of this study are available from the corresponding author upon reasonable request.

Funding

This work was supported by MITACS Canada under Grant [IT12425]; Origin Materials; and the Faculty of Engineering at the University of Western Ontario.

Declaration of Competing Interest

The authors report there are no competing interests to declare.

References

1. Khan TA, Saud AS, Jamari SS, Rahim MHA, Park JW, Kim HJ. Hydrothermal carbonization of lignocellulosic biomass for carbon rich material preparation: A review. *Biomass Bioenergy* **2019**, *130*, 105384. DOI:10.1016/j.biombioe.2019.105384
2. Liu Z, Zhang F-S. Removal of lead from water using biochars prepared from hydrothermal liquefaction of biomass. *J. Hazard. Mater.* **2009**, *167*, 933–939. DOI:10.1016/j.jhazmat.2009.01.085
3. Gronwald M, Vos C, Helfrich M, Don A. Stability of pyrochar and hydrochar in agricultural soil - a new field incubation method. *Geoderma* **2016**, *284*, 85–92. DOI:10.1016/j.geoderma.2016.08.019
4. Paneque M, Knicker H, Kern J, De la Rosa JM. Hydrothermal Carbonization and Pyrolysis of Sewage Sludge: Effects on Lolium perenne Germination and Growth. *Agronomy* **2019**, *9*, 363. DOI:10.3390/agronomy9070363
5. Wang Y, Qiu L, Zhu M, Sun G, Zhang T, Kang K. Comparative Evaluation of Hydrothermal Carbonization and Low Temperature Pyrolysis of Eucommia ulmoides Oliver for the Production of Solid Biofuel. *Sci. Rep.* **2019**, *9*, 5535. DOI:10.1038/s41598-019-38849-4
6. Titirici M-M, Thomas A, Antonietti M. Back in the black: Hydrothermal carbonization of plant material as an efficient chemical process to treat the CO_2 problem? *New J. Chem.* **2007**, *31*, 787–789. DOI:10.1039/b616045j
7. Hosny M, Fawzy M. Sustainable synthesis of a novel hydrothermally carbonized AuNPs-hydrochar nanocomposite for the photocatalytic degradation of cephalexin. *Biomass Conv. Bioref.* **2024**, *14*, 30559–30576. DOI:10.1007/s13399-023-04893-4
8. Buss W, Mašek O. Mobile organic compounds in biochar—A potential source of contamination—Phytotoxic effects on cress seed (*Lepidium sativum*) germination. *J. Environ. Manag.* **2014**, *137*, 111–119. DOI:10.1016/j.jenvman.2014.01.045
9. Fang J, Zhan L, Ok YS, Gao B. Minireview of potential applications of hydrochar derived from hydrothermal carbonization of biomass. *J. Ind. Eng. Chem.* **2018**, *57*, 15–21. DOI:10.1016/j.jiec.2017.08.026

10. Rafatullah M, Sulaiman O, Hashim R, Ahmad A. Adsorption of methylene blue on low-cost adsorbents: A review. *J. Hazard. Mater.* **2010**, *177*, 70–80. DOI:10.1016/j.jhazmat.2009.12.047
11. Fierro V, Torné-Fernández V, Montané D, Celzard A. Adsorption of phenol onto activated carbons having different textural and surface properties. *Microporous Mesoporous Mater.* **2008**, *111*, 276–284. DOI:10.1016/j.micromeso.2007.08.002
12. Kong L, Diao Z, Chang X, Xiong Y, Chen D. Synthesis of recoverable and reusable granular MgO-SCCA-Zn hybrid ozonation catalyst for degradation of methylene blue. *J. Environ. Chem. Eng.* **2016**, *4*, 4385–4391. DOI:10.1016/j.jece.2016.10.002
13. Chegini G, Briens C, Pjontek D. Production and characterization of adsorbents from a hydrothermal char by pyrolysis, carbon dioxide and steam activation. *Biomass Conv. Bioref.* **2023**, *13*, 13163–13179. DOI:10.1007/s13399-022-02439-8
14. Figueiredo JL, Pereira MFR, Freitas MMA, Órfão JJM. Modification of the surface chemistry of activated carbons. *Carbon* **1999**, *37*, 1379–1389. DOI:10.1016/S0008-6223(98)00333-9
15. Bhatnagar A, Hogland W, Marques M, Sillanpää M. An overview of the modification methods of activated carbon for its water treatment applications. *Chem. Eng. J.* **2013**, *219*, 499–511. DOI:10.1016/j.cej.2012.12.038
16. Stavropoulos GG, Samaras P, Sakellaropoulos GP. Effect of activated carbons modification on porosity, surface structure and phenol adsorption. *J. Hazard. Mater.* **2008**, *151*, 414–421. DOI:10.1016/j.jhazmat.2007.06.005
17. Soudani N, Souissi-najar S, Ouederni A. Influence of Nitric Acid Concentration on Characteristics of Olive Stone Based Activated Carbon. *Chin. J. Chem. Eng.* **2013**, *21*, 1425–1430. DOI:10.1016/S1004-9541(13)60638-2
18. Nguyen DH, Tran HN, Chao H-P, Lin CC. Effect of nitric acid oxidation on the surface of hydrochars to sorb methylene blue: An adsorption mechanism comparison. *Adsorpt. Sci. Technol.* **2019**, *37*, 607–622. DOI:10.1177/0263617419867519
19. Güzel F, Sayğılı H, Akkaya Sayğılı G, Koyuncu F, Yılmaz C. Optimal oxidation with nitric acid of biochar derived from pyrolysis of weeds and its application in removal of hazardous dye methylene blue from aqueous solution. *J. Clean. Prod.* **2017**, *144*, 260–265. DOI:10.1016/j.jclepro.2017.01.029
20. Gokce Y, Aktas Z. Nitric acid modification of activated carbon produced from waste tea and adsorption of methylene blue and phenol. *Appl. Surf. Sci.* **2014**, *313*, 352–359. DOI:10.1016/j.apsusc.2014.05.214
21. Mourão PAM, Laginhas C, Custódio F, Nabais JMV, Carrott PJM, Carrott MMLR. Influence of oxidation process on the adsorption capacity of activated carbons from lignocellulosic precursors. *Fuel Process. Technol.* **2011**, *92*, 241–246. DOI:10.1016/j.fuproc.2010.04.013
22. Yakout SM. Monitoring the Changes of Chemical Properties of Rice Straw–Derived Biochars Modified by Different Oxidizing Agents and Their Adsorptive Performance for Organics. *Bioremediation J.* **2015**, *19*, 171–182. DOI:10.1080/10889868.2015.1029115
23. El-Hendawy ANA. Influence of HNO3 oxidation on the structure and adsorptive properties of corncob-based activated carbon. *Carbon* **2003**, *41*, 713–722. DOI:10.1016/S0008-6223(03)00029-0
24. Ok YS, Tsang DCW, Bolan N, Novak JM. *Biochar from Biomass and Waste: Fundamentals and Applications*; Elsevier: San Diego, CA, USA, 2018.
25. Enaime G, Baçaoui A, Yaacoubi A, Lübken M. Biochar for Wastewater Treatment—Conversion Technologies and Applications. *Appl. Sci.* **2020**, *10*, 3492. DOI:10.3390/app10103492
26. Girgis BS, Soliman AM, Fathy NA. Development of micro-mesoporous carbons from several seed hulls under varying conditions of activation. *Microporous Mesoporous Mater.* **2011**, *142*, 518–525. DOI:10.1016/j.micromeso.2010.12.044
27. Qambrani NA, Rahman MM, Won S, Shim S, Ra C. Biochar properties and eco-friendly applications for climate change mitigation, waste management, and wastewater treatment: A review. *Renew. Sustain. Energy Rev.* **2017**, *79*, 255–273. DOI:10.1016/j.rser.2017.05.057
28. Ahmad M, Rajapaksha AU, Lim JE, Zhang M, Bolan N, Mohan D, et al. Biochar as a sorbent for contaminant management in soil and water: A review. *Chemosphere* **2014**, *99*, 19–33. DOI:10.1016/j.chemosphere.2013.10.071
29. Rosales E, Meijide J, Pazos M, Sanromán MA. Challenges and recent advances in biochar as low-cost biosorbent: From batch assays to continuous-flow systems. *Bioresour. Technol.* **2017**, *246*, 176–192. DOI:10.1016/j.biortech.2017.06.084
30. Tran HN, You SJ, Chao HP. Insight into adsorption mechanism of cationic dye onto agricultural residues-derived hydrochars: Negligible role of π-π interaction. *Korean J. Chem. Eng.* **2017**, *34*, 1708–1720. DOI:10.1007/s11814-017-0056-7
31. Dong F-X, Yan L, Zhou X-H, Huang ST, Liang JY, Zhang WX, et al. Simultaneous adsorption of Cr(VI) and phenol by biochar-based iron oxide composites in water: Performance, kinetics and mechanism. *J. Hazard. Mater.* **2021**, *416*, 125930. DOI:10.1016/j.jhazmat.2021.125930
32. Villacañas F, Pereira MFR, Órfão JJM, Figueiredo JL. Adsorption of simple aromatic compounds on activated carbons. *J. Colloid Interface Sci.* **2006**, *293*, 128–136. DOI:10.1016/j.jcis.2005.06.032
33. Chen JP, Wu S. Acid/Base-Treated Activated Carbons: Characterization of Functional Groups and Metal Adsorptive Properties. *Langmuir* **2004**, *20*, 2233–2242. DOI:10.1021/la0348463

34. Allwar A, Hartati R, Fatimah I. Effect of nitric acid treatment on activated carbon derived from oil palm shell. *AIP Conf. Proc.* **2017**, *1821*, 020129. DOI:10.1063/1.4978202
35. Balistrieri LS, Murray JW. The surface chemistry of goethite (alpha-FeOOH) in major ion seawater. *Am. J. Sci.* **1981**, *281*, 788–806. DOI:10.2475/ajs.281.6.788
36. Nouha S, Souad NS, Abdelmottalab O. ENHANCED ADSORPTION OF PHENOL USING ALKALINE MODIFIED ACTIVATED CARBON PREPARED FROM OLIVE STONES. *J. Chil. Chem. Soc.* **2019**, *64*, 4352–4359. DOI:10.4067/s0717-97072019000104352
37. Goertzen SL, Thériault KD, Oickle AM, Tarasuk AC, Andreas HA. Standardization of the Boehm titration. Part I. CO_2 expulsion and endpoint determination. *Carbon* **2010**, *48*, 1252–1261. DOI:10.1016/j.carbon.2009.11.050
38. Rafiq M, Ahmed A, Usman M, Ullah R, Gao F, Mateen M, et al. Efficient heterogeneous activation of peroxymonosulfate by manganese-doped $LaCoO_3$ perovskites for metronidazole degradation: A mechanistic study and reaction pathways. *J. Environ. Chem. Eng.* **2023**, *11*, 111608. DOI:10.1016/j.jece.2023.111608
39. Rafiq M, Ullah R, Ahmed A, Liu X, Usman M, Cao Q, et al. Highly efficient degradation of norfloxacin by using Co_3O_4-CeO_2 as a heterogeneous catalyst through peroxymonosulfate activation: Characterization, catalytic performance and mechanism. *J. Water Process Eng.* **2025**, *71*, 107167. DOI:10.1016/j.jwpe.2025.107167
40. Sadegh-Zadeh F, Samsuri AW, Seh-Bardan BJ, Emadi M. The effects of acidic functional groups and particle size of biochar on Cd adsorption from aqueous solutions. *Desalination Water Treat.* **2017**, *66*, 309–319. DOI:10.5004/dwt.2017.20216
41. Li X, Shen Q, Zhang D, Mei X, Ran W, Xu Y, et al. Functional Groups Determine Biochar Properties (pH and EC) as Studied by Two-Dimensional 13C NMR Correlation Spectroscopy. *PLoS ONE* **2013**, *8*, e65949. DOI:10.1371/journal.pone.0065949
42. Chun Y, Sheng G, Chiou CT, Xing B. Compositions and Sorptive Properties of Crop Residue-Derived Chars. *Environ. Sci. Technol.* **2004**, *38*, 4649–4655. DOI:10.1021/es035034w
43. Jin J, Li S, Peng X, Liu W, Zhang C, Yang Y, et al. HNO_3 modified biochars for uranium (VI) removal from aqueous solution. *Bioresour. Technol.* **2018**, *256*, 247–253. DOI:10.1016/j.biortech.2018.02.022
44. Fang J, Gao B, Chen J, Zimmerman AR. Hydrochars derived from plant biomass under various conditions: Characterization and potential applications and impacts. *Chem. Eng. J.* **2015**, *267*, 253–259. DOI:10.1016/j.cej.2015.01.026
45. Kim K, Zhu P, Li N, Ma X, Chen Y. Characterization of oxygen containing functional groups on carbon materials with oxygen K-edge X-ray absorption near edge structure spectroscopy. *Carbon* **2011**, *49*, 1745–1751. DOI:10.1016/j.carbon.2010.12.060
46. Trompowsky PM, Benites VDM, Madari BE, Pimenta AS, Hockaday WC, Hatcher PG. Characterization of humic like substances obtained by chemical oxidation of eucalyptus charcoal. *Org. Geochem.* **2005**, *36*, 1480–1489. DOI:10.1016/j.orggeochem.2005.08.001
47. Chen B, Zhou D, Zhu L. Transitional Adsorption and Partition of Nonpolar and Polar Aromatic Contaminants by Biochars of Pine Needles with Different Pyrolytic Temperatures. *Environ. Sci. Technol.* **2008**, *42*, 5137–5143. DOI:10.1021/es8002684
48. Fiol N, Villaescusa I. Determination of sorbent point zero charge: usefulness in sorption studies. *Environ. Chem. Lett.* **2009**, *7*, 79–84. DOI:10.1007/s10311-008-0139-0
49. Tehrani-Bagha AR, Balchi T. Catalytic Wet Peroxide Oxidation. In *Advanced Oxidation Processes for Wastewater Treatment: Emerging Green Chemical Technology*; Elsevier Inc.: Amsterdam, The Netherlands, 2018; pp. 375–402. DOI:10.1016/B978-0-12-810499-6.00012-7
50. Mei Y, Bai Y, Wang L. Effect of pH on binding of pyrene to hydrophobic fractions of dissolved organic matter (DOM) isolated from lake water. *Acta Geochim.* **2016**, *35*, 288–293. DOI:10.1007/s11631-016-0094-6
51. Belhachemi M, Addoun F. Effect of Heat Treatment on the Surface Properties of Activated Carbons. *J. Chem.* **2011**, *8*, 992–999. DOI:10.1155/2011/649254
52. Sajjadi B, Chen WY, Egiebor NO. A comprehensive review on physical activation of biochar for energy and environmental applications. *Rev. Chem. Eng.* **2019**, *35*, 735–776. DOI:10.1515/revce-2017-0113
53. Ncibi MC, Mahjoub B, Seffen M. Kinetic and equilibrium studies of methylene blue biosorption by *Posidonia oceanica* (L.) fibres. *J. Hazard. Mater.* **2007**, *139*, 280–285. DOI:10.1016/j.jhazmat.2006.06.029
54. Lowell S, Shields JE, Thomas MA, Thommes M. Characterization of porous solids and powders: Surface area, pore size, and density. *Choice Rev. Online* **2005**, *42*, 42–5288–42–5288. DOI:10.5860/CHOICE.42-5288
55. Lorenc-Grabowska E. Effect of micropore size distribution on phenol adsorption on steam activated carbons. *Adsorption* **2016**, *22*, 599–607. DOI:10.1007/s10450-015-9737-x

56. Aringheieri R, Pardini G, Gisperet M, Sole A. Testing a simple methylene blue method for surface area estimation in soils. *Agrochimica* **1992**, *36*, 224–232. Available online: https://agris.fao.org/search/en/providers/122556/records/6477576cf2e6fe92b36593f1 (accessed on 10 February 2021).
57. Mohd Shaid MSH, Zaini MAA, Nasri NS. Evaluation of methylene blue dye and phenol removal onto modified CO_2-activated pyrolysis tyre powder. *J. Clean. Prod.* **2019**, *223*, 487–498. DOI:10.1016/j.jclepro.2019.03.097
58. Le GTT, Chanlek N, Manyam J, Opaprakasit P, Grisdanurak N, Sreearunothai P. Insight into the ultrasonication of graphene oxide with strong changes in its properties and performance for adsorption applications. *Chem. Eng. J.* **2019**, *373*, 1212–1222. DOI:10.1016/j.cej.2019.05.108
59. Peiris C, Nayanathara O, Navarathna CM, Jayawardhana Y, Nawalage S, Burk G, et al. The influence of three acid modifications on the physicochemical characteristics of tea-waste biochar pyrolyzed at different temperatures: A comparative study. *RSC Adv.* **2019**, *9*, 17612–17622. DOI:10.1039/C9RA02729G
60. Franz M, Arafat HA, Pinto NG. Effect of chemical surface heterogeneity on the adsorption mechanism of dissolved aromatics on activated carbon. *Carbon* **2000**, *38*, 1807–1819. DOI:10.1016/S0008-6223(00)00012-9
61. Kipling JJ, Wilson RB. Adsorption of methylene blue in the determination of surface areas. *J. Appl. Chem.* **1960**, *10*, 109–113. DOI:10.1002/jctb.5010100303
62. Santamarina JC, Klein KA, Wang YH, Prencke E. Specific surface: determination and relevance. *Can. Geotech. J.* **2002**, *39*, 233–241. DOI:10.1139/t01-077
63. Terzyk AP. Further insights into the role of carbon surface functionalities in the mechanism of phenol adsorption. *J. Colloid Interface Sci.* **2003**, *268*, 301–329. DOI:10.1016/S0021-9797(03)00690-8
64. Vidic RD, Tessmer CH, Uranowski LJ. Impact of surface properties of activated carbons on oxidative coupling of phenolic compounds. *Carbon* **1997**, *35*, 1349–1359. DOI:10.1016/S0008-6223(97)00071-7
65. Radovic LR, Silva IF, Ume JI, Menéndez JA, Leon CALY, Scaroni AW. An experimental and theoretical study of the adsorption of aromatics possessing electron-withdrawing and electron-donating functional groups by chemically modified activated carbons. *Carbon* **1997**, *35*, 1339–1348. DOI:10.1016/S0008-6223(97)00072-9
66. Dąbrowski A, Podkościelny P, Hubicki Z, Barczak M. Adsorption of phenolic compounds by activated carbon—A critical review. *Chemosphere* **2005**, *58*, 1049–1070. DOI:10.1016/j.chemosphere.2004.09.067
67. Moreno-Castilla C. Adsorption of organic molecules from aqueous solutions on carbon materials. *Carbon* **2004**, *42*, 83–94. DOI:10.1016/j.carbon.2003.09.022
68. Coughlin RW, Ezra FS. Role of surface acidity in the adsorption of organic pollutants on the surface of carbon. *Environ. Sci. Technol.* **1968**, *2*, 291–297. DOI:10.1021/es60016a002
69. Salame II, Bandosz TJ. Role of surface chemistry in adsorption of phenol on activated carbons. *J. Colloid Interface Sci.* **2003**, *264*, 307–312. DOI:10.1016/S0021-9797(03)00420-X
70. Nevskaia DM, Santianes A, Muñoz V, Guerrero-Ruíz A. Interaction of aqueous solutions of phenol with commercial activated carbons: an adsorption and kinetic study. *Carbon* **1999**, *37*, 1065–1074. DOI:10.1016/S0008-6223(98)00301-7
71. Álvarez PM, García-Araya JF, Beltrán FJ, Masa FJ, Medina F. Ozonation of activated carbons: Effect on the adsorption of selected phenolic compounds from aqueous solutions. *J. Colloid Interface Sci.* **2005**, *283*, 503–512. DOI:10.1016/j.jcis.2004.09.014
72. Haydar S, Ferro-García MA, Rivera-Utrilla J, Joly JP. Adsorption of p-nitrophenol on an activated carbon with different oxidations. *Carbon* **2003**, *41*, 387–395. DOI:10.1016/S0008-6223(02)00344-5
73. Pereira MFR, Soares SF, Órfão JJM, Figueiredo JL. Adsorption of dyes on activated carbons: influence of surface chemical groups. *Carbon* **2003**, *41*, 811–821. DOI:10.1016/S0008-6223(02)00406-2
74. Oyekanmi AA, Ahmad A, Hossain K, Rafatullah M. Adsorption of Rhodamine B dye from aqueous solution onto acid treated banana peel: Response surface methodology, kinetics and isotherm studies. *PLoS ONE* **2019**, *14*, e0216878. DOI:10.1371/journal.pone.0216878
75. Khan TA, Khan EA, Shahjahan. Adsorptive uptake of basic dyes from aqueous solution by novel brown linseed deoiled cake activated carbon: Equilibrium isotherms and dynamics. *J. Environ. Chem. Eng.* **2016**, *4*, 3084–3095. DOI:10.1016/j.jece.2016.06.009
76. Órfão JJM, Silva AIM, Pereira JCV, Barata SA, Fonseca IM, Faria PCC, et al. Adsorption of a reactive dye on chemically modified activated carbons—Influence of pH. *J. Colloid Interface Sci.* **2006**, *296*, 480–489. DOI:10.1016/j.jcis.2005.09.063
77. Acevedo B, Rocha RP, Pereira MFR, Figueiredo JL, Barriocanal C. Adsorption of dyes by ACs prepared from waste tyre reinforcing fibre. Effect of texture, surface chemistry and pH. *J. Colloid Interface Sci.* **2015**, *459*, 189–198. DOI:10.1016/j.jcis.2015.07.068